GEOPHYSICS, VOL. 67, NO. 2 (MARCH-APRIL 2002); P. 405–412, 9 FIGS., 4 TABLES.
10.1190/1.1468600

Acoustic measurements in unconsolidated sands at low effective pressure and overpressure detection

Manika Prasad*

ABSTRACT

Shallow water flows and over-pressured zones are a major hazard in deepwater drilling projects. Their detection prior to drilling would save millions of dollars in lost drilling costs. I have investigated the sensitivity of seismic methods for this purpose. Using P-wave information alone can be ambiguous, because a drop in P-wave velocity (V_p) can be caused both by overpressure and by presence of gas. The ratio of P-wave velocity to S-wave velocity (V_p/V_s), which increases with overpressure and decreases with gas saturation, can help differentiate between the two cases. Since P-wave velocity in a suspension is slightly below that of the suspending fluid and $V_s = 0$, V_p/V_s and Poisson's ratio must increase exponentially as a load-bearing sediment approaches a state of suspension. On the other hand, presence of gas will also decrease V_p but V_s will remain unaffected and V_p/V_s will decrease. Analyses of ultrasonic P- and S-wave velocities in sands show that the V_p/V_s ratio, especially at low effective pressures, decreases rapidly with pressure. At very low pressures, V_p/V_s values can be as large as 100 and higher. Above pressures greater than 2 MPa, it plateaus and does not change much with pressure. There is significant change in signal amplitudes and frequency of shear waves below 1 MPa. The current ultrasonic data shows that V_p/V_s values can be invaluable indicators of low differential pressures.

INTRODUCTION

In deeper waters, shallow water flows (SWF) and sand production are major operation and exploration hazards. SWF zones are generally located between 400 and 2100 m water depths and at depths between the seabed and about 1220 m below the mudline (Huffman and Castagna, 1999, 2000). Under a large water column, pore pressures are high and the sediments can be undercompacted. The high pore pressures decrease the total differential pressure, P_d, ($P_d = P_{\text{overburden}} - P_{\text{pore}}$) acting on the sediment. At such conditions of low differential stresses, sediments (for example, sands in the Gulf of Mexico) are very loosely packed. In the case of Gulf of Mexico, shaly sediments and rapid sedimentation prevent the underlying sediments from draining and make overpressure generation possible.

Seismic velocities or interval transit times are often used for remote detection and prediction of high pore-pressure regions (Hottmann and Johnson, 1965; Pennebaker, 1970; Dutta, 1987; Pilkington, 1988). Numerous empirical models exist to link P-wave velocity (V_p) to overpressure. However, using P-wave information alone can give ambiguous results: both overpressure and pressure of gas can decrease V_p. Since S-wave velocity (V_s) decreases with overpressure but is unaffected by change in saturation, V_p/V_s, which will increase with overpressure and decrease with presence of gas, can be used to distinguish between them. A systematic laboratory analysis of P- and S-wave signatures in unconsolidated sediments at low effective pressures is lacking. Theoretically, it has been shown that at or above critical porosity, as the sediment turns into a suspension, V_p will be given by the Wood's equation for suspensions, the sediment will loose shear strength, and V_s will decrease to zero (Nur et al., 1995). Hamilton (1971a, b) and Huffman and Castagna (1999) have suggested that the corresponding V_p-V_s ratio should show a large change as differential pressure goes to zero at porosity near the critical porosity. It stands to reason that, at low effective pressures, the corresponding shear attenuation should be very high and P-wave quality factor–S-wave quality factor (Q_p-Q_s) ratio trends should track V_p-V_s ratio trends.

P- and S-wave velocity data in unconsolidated sediments, especially at low differential pressures is sparse. The exact nature of V_p/V_s at low pressures remains to be investigated. In this paper, I present velocity and attenuation data in sands at low (0 to 1 MPa) differential pressures. The low-pressure laboratory data is compared to similar data at higher pressures from Prasad and Meissner (1992), and Yin (1992). The relation between V_p/V_s and pressure will help us to predict and map overpressured regions from remote measurements.

Published on Geophysics Online January 7, 2002. Manuscript received by the Editor May 18, 2000; revised manuscript received February 28, 2001.
*Stanford University, Geophysics Department, 397 Panama Mall, Stanford, California 94305. E-mail: manika.prasad@stanford.edu.

DATA AND SAMPLES USED

Table 1 lists the data used in this study, which spanned a frequency range from megahertz (Yin, 1992; this study) to kilohertz (Prasad and Meissner, 1992; Ayers and Theilen, 1999). The data and sample selection was made keeping simple systems in mind. Thus, only sand data was chosen. The second criterion was pressure: only data that contained low-pressure V_p and V_s information was chosen. The third criterion was to choose only fully saturated measurements. The experiments in this study honored all three criteria: clean beach sands (grain size 250–550 μm), fully saturated measurements up to 1 MPa. Future studies will include additional effects of grain size and sorting (Zimmer et al., 2002).

EXPERIMENTAL SETUP

The pulse-transmission experimental setup (Figure 1) consisted of a digital oscilloscope (Tektronix TDS 420A) and a pulse generator (Panametrics 5052PR). Panametrics transducers (1-MHz principal frequency, 25.4-mm diameter) were used to generate *P*- and *S*-waves. The sand was wetted with the pore fluid and then rained in the pore fluid contained in a rubber jacket to a height of about 12 mm. This procedure prevented air bubbles from getting trapped and ensured full saturation. Transducers contained in holders were placed on each side of the jacket. Pore fluid was not allowed to escape during the measurements. Sample length was measured at each step using calipers (accuracy = 0.1 mm). A hand press was used to generate the small pressures required for this study. Force on the sample was measured with a load cell placed between the transducer and the sample. Pressure was calculated from this force divided by the area of the transducer in contact with the sample.

Traveltime was measured after digitizing each trace with 1024 points at a maximum time sweep of 200 μs, thus allowing a time resolution of about 0.2 μs. Error in velocity measurement is estimated to be around 1% due to operator error in picking first arrival. The system delay time was measured by taking head-to-head time. Frequency analysis were made by fast Fourier transforms of windowed signals using a cosine taper.

RESULTS

I first recap some key results from Prasad and Meissner (1992), who showed that V_p, V_s, Q_p, and Q_s were grain size and pressure dependent. Figure 2 shows V_p, V_s, dynamic shear (μ), and bulk (K) moduli, and Q_p and Q_s variations with pressure for two water-saturated sands (from Prasad and Meissner, 1992): coarse grained (open circles) with a median grain size = 550 μm, and fine grained (closed circles) with a median grain size = 220 μm The plots show a difference in the pressure dependence between *P*- and *S*-waves; pressure appears to have a greater effect on shear waves (about 300%) than on compressional waves (about 20%). These characteristics were used to analyze pressure-sensitive seismic attributes in sands.

Figures 3a–3d show V_p/V_s, Q_p/Q_s, Poisson's ratio, and K/μ, respectively, as a function of pressure, calculated from Prasad's data (Prasad, 1988). All three quantities decrease exponentially with pressure. To better visualize the changes at low pressures, Figures 3e–3h show the same results zoomed in at low pressures (up to 2 MPa).

Although the results in Figure 3 show an exponential change with pressure, due to a paucity of information, the exact nature of this change at low pressures is largely unknown. The current experiment was conducted at very low effective pressures (up to 1 MPa) to explore this low-pressure regime. Figure 4a shows typical *P*-wave signals, and Figure 4b shows their normalized power spectra measured through the sand at different pressures: red is lowest and blue is highest pressure. The different red colored signals were taken before (solid) and after (hashed) the loading process. The difference between the two signals at the same pressure shows that significant hysteresis is to be expected in such studies. The corresponding length change was from 11 mm to 8 mm.

S-waves showed very dramatic changes in signal properties with pressure. Figure 5 shows typical *S*-wave signals measured in the sands at different pressures. As in Figure 4, red is lowest and blue is highest pressure. In addition to the changes seen in *P*-waves, we can see a drastic change in frequency of the *S*-wave signals with pressure.

To better visualize these changes in shear waves, the signals and their normalized power spectra measured at low pressures are shown in Figures 6a and 6b, respectively. Note that for ease of comparison, the signals are plotted so that their arrival times are almost coincident. A large change in amplitude and in wavelength is obvious between 0 and 0.36 MPa. Although

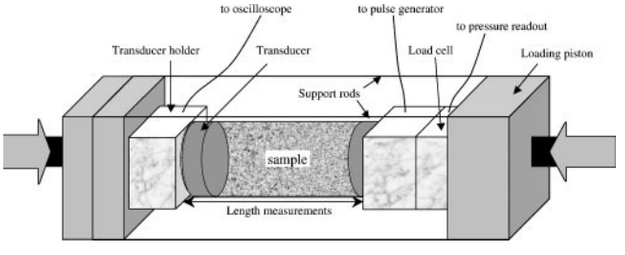

FIG. 1. Sketch of the experimental pulse-transmission setup.

Table 1. Type and source of the data used in this study.

	Experiment	Sediment	Frequency	Source
1.	Laboratory	Various grain sized sand	100 kHz	Prasad and Meissner (1992)
2.	Laboratory	Ottawa sand	1 MHz	Yin (1992)
3.	Laboratory	Marine sediments	10–20 kHz	Ayers and Theilen (1999)
4.	Laboratory	Sands	1 MHz	This study
5.	Empirical	Marine sediments	Not available	Hamilton (1971a, b)

some changes might be a result of better coupling with pressure, the extremely high attenuation of shear waves at low pressures is an indication that the sand is close to a state of suspension. In such a state, the sediment will have very low shear strength and will act as a low-pass filter for shear waves. *P*-waves are not affected in the same way.

The most significant changes in *P*- and *S*-wave amplitude, frequency, and wavelength corresponding to a pressure

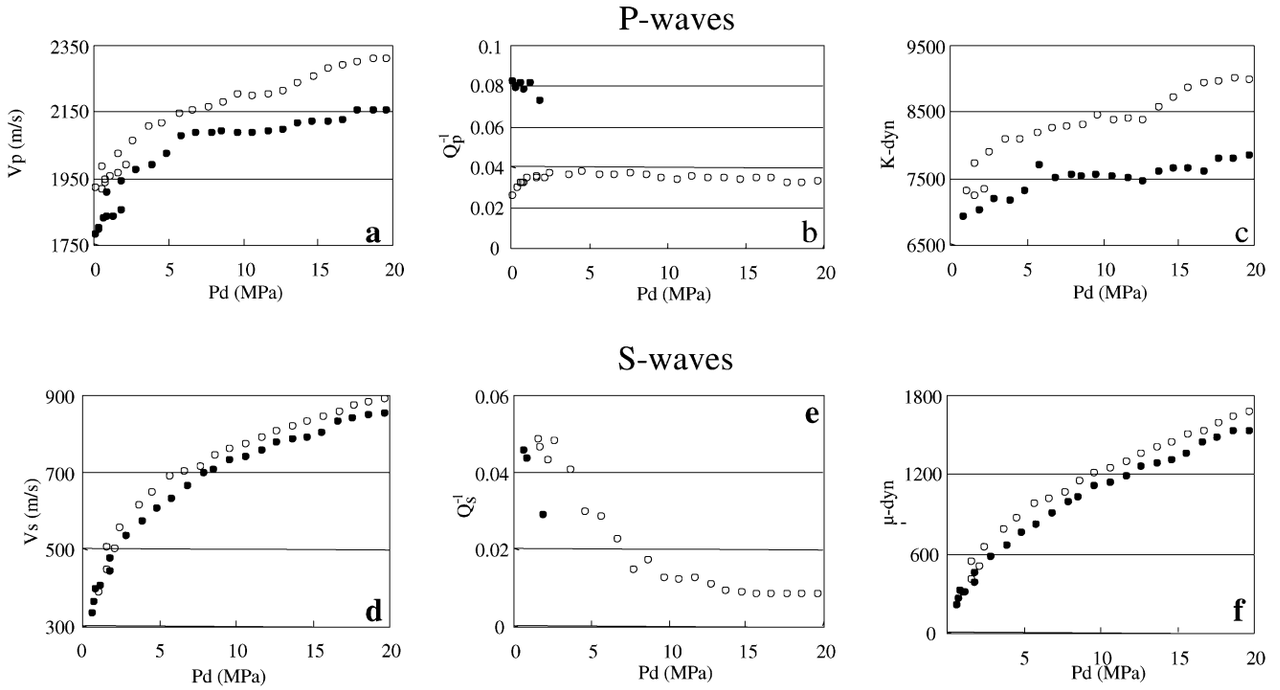

FIG. 2. Example results from Prasad and Meissner (1992). *P*- and *S*-wave velocities (V_p in a, V_s in d), quality factors (Q_p in b, Q_s in e), and dynamic bulk (*K-dyn* in c) and shear (μ-*dyn* in f) moduli results for two water-saturated sands with different grain sizes are plotted: open circles = fine grained (mean diameter = 220 μm), solid circles = coarse grained (mean diameter = 500 μm).

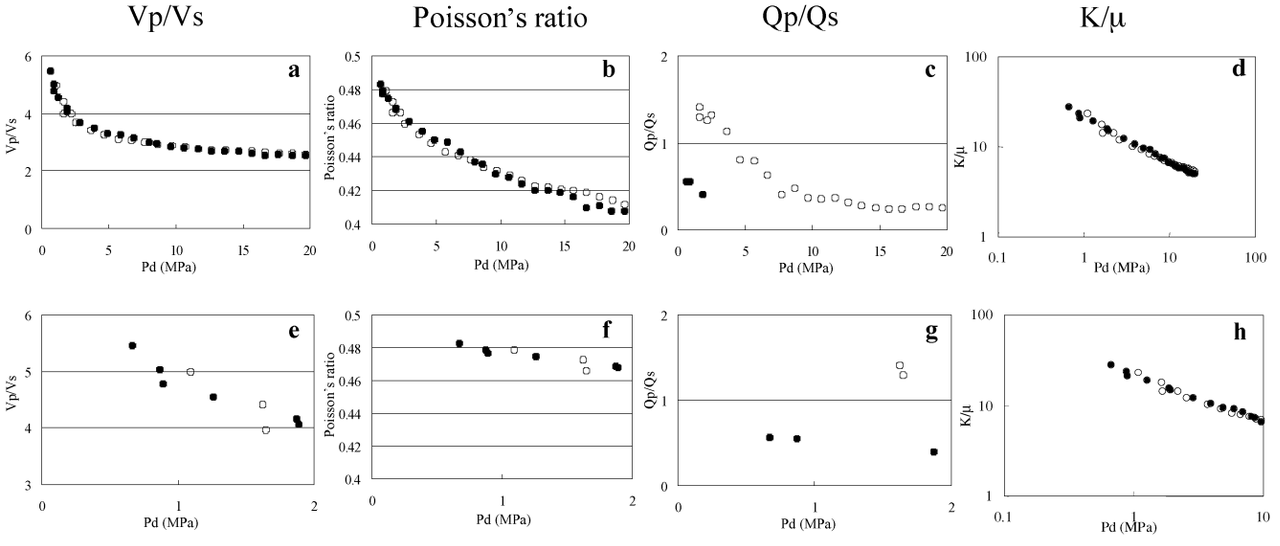

FIG. 3. V_p/V_s (a and e), Poisson's ratio (3 and f), Q_p/Q_s (c and g), and *K-dyn*/μ-*dyn* (d and h) calculated from Prasad (1988). The results are from two water-saturated sands with different grain sizes: open circles = fine grained (mean diameter = 220 μm), solid circles = coarse grained (mean diameter = 500 μm). The first row (a–d) shows all the data to 20 MPa, the second row plots (e–h) show an expanded view of changes at low pressures up to 2 MPa (to 10 MPa for K/μ). An exponential decrease in all three parameters with pressure is observed.

change from 0 to 0.9 MPa are summarized in Table 2. The changes observed in shear-wave signals corresponding to a pressure change from 0 to 1.2 MPa are at least equal, if not larger than those recorded for the compressional waves. The amplitude change is comparable in both cases. Frequency change is much larger in *S*-waves (over 100%) than in *P*-waves (8%).

DISCUSSION

Figure 7 shows V_p/V_s as a function of pressure for the data collected in this study along with data from Prasad and Meissner (1992) for sands, from Ayers and Theilen (1999) for marine sediments, and the empirical trends for sand and shale given by Hamilton (1971a, b). The data used for these figures is given in Table 3. The figure shows an exponential increase in V_p/V_s ratio with pressure reduction; V_p/V_s increases from about 2 at 5 MPa to above 10 at 0.5 MPa. The details of the V_p/V_s change at low pressures (Figure 7b) show that the maximum change occurs between 0 and 2 MPa. The values calculated from Ayers and Theilen (1999) data was measured at low frequency (about 10–20 kHz) using low-frequency bender element transducers. These two data points with high V_p/V_s ratio values of 70 and 200 agree with the general data trend.

V_p/V_s values for all the laboratory data in Table 3 is combined in Figure 8. The solid line is an empirical fit to the data ($V_p/V_s = 5.6014 \times P_d^{-0.2742}$, with P_d in megapascals). The coefficient of regression for this fit (R^2) is about 0.8. This is in general agreement with results of Huffman and Castagna (1999, 2000), although according to their prediction, V_p/V_s is expected to rapidly decrease to values below 4 by 0.1 MPa. The current study shows that high values of V_p/V_s can be expected up to 2 MPa.

Velocity and attenuation data can be useful tools to distinguish between different lithologies and between overpressure and saturation effects. Whereas both overpressure and saturation cause a decrease in V_p, V_s is unaffected by saturation state and decreases with overpressure. Thus, V_p/V_s ratio will move in different directions. Figure 9 shows data for a sandstone (from

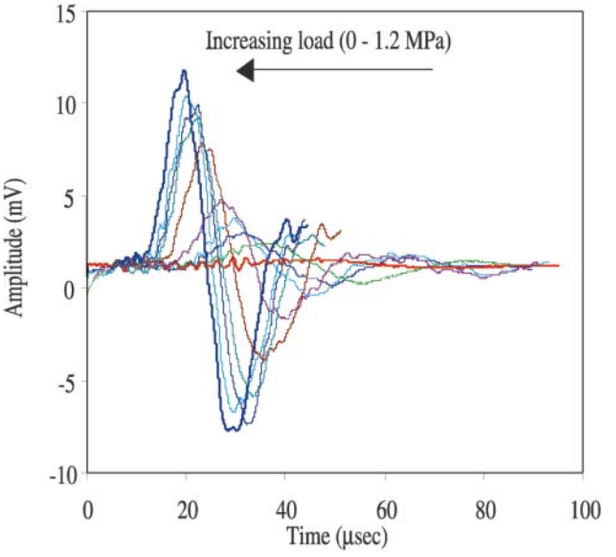

FIG. 5. Typical *S*-wave signals through water-saturated sands at low effective pressures, up to 1.2 MPa. Red curve (hashed) was made at 0 MPa, and solid blue curve at 1.2 MPa. During the loading experiment, no *S*-signal could be recorded. It was visible only after the loading process was completed and the sand had been precompacted.

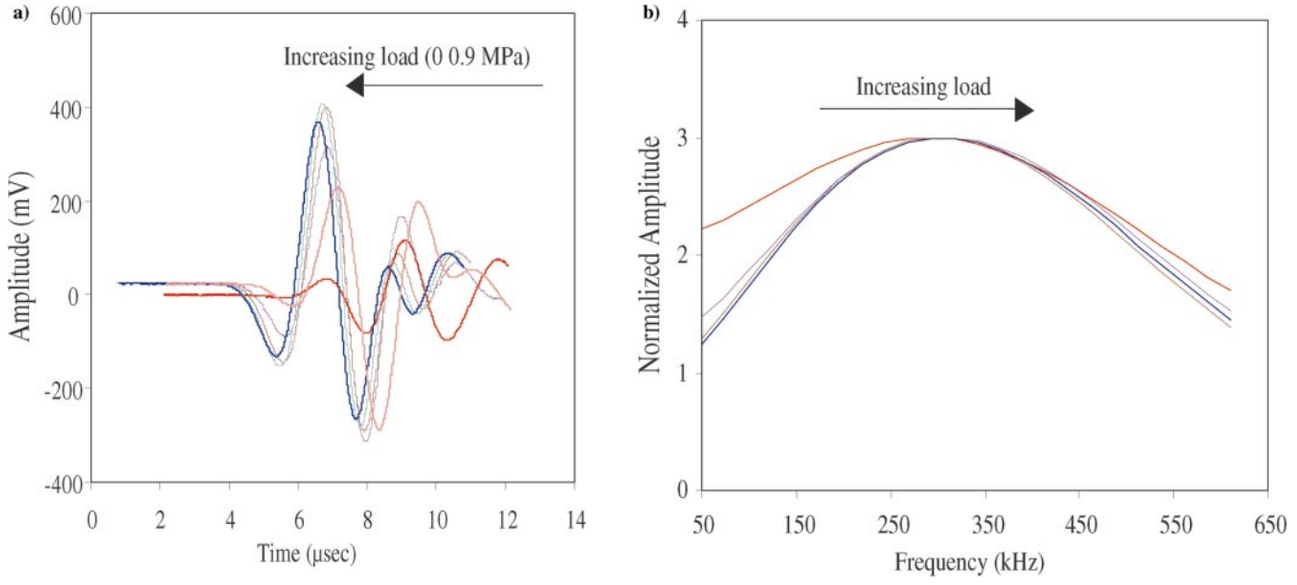

FIG. 4. Typical *P*-wave signals (a) and their normalized Fourier frequency spectra (b) through water-saturated sands at low effective pressures, up to 0.9 MPa. Red curves were made at 0 MPa, and blue curves at 0.9 MPa. The two red curves, made before (solid line) and after (hashed line), the loading process show the amount of hysteresis in the sample.

Prasad, 2001) and saturated sands (from Prasad and Meissner, 1992). The sands can be separated from sandstones on this Q_p/Q_s versus $(V_p/V_s)^2$ plot. The effect of increasing pore pressure (decreasing differential pressure) is to increase both Q_p/Q_s and V_p/V_s ratios. A practical application of these results can be to detect SWF zones. Table 4 gives values of different seismic attributes in gas-saturated and water-saturated sands as a function of pressure. The effect of pressure on the normal incidence P-wave reflectivity (NI) and the Poisson reflectivity

Table 2. Comparison of changes in amplitude and frequency of *P*- and *S*-wave signals as a function of pressure. The frequency was derived from fast Fourier transform of each signal.

Wave property	Pressure = 0 MPa	Pressure = 0.9 MPa
P-wave amplitude	−6.8, 33.0 mV	−131.6, 368.8 mV
S-wave amplitude	1.60, 1.09 mV	11.78, −7.74 mV
P-wave frequency	293 kHz	317 kHz
S-wave frequency	14.7 kHz	36.6 kHz

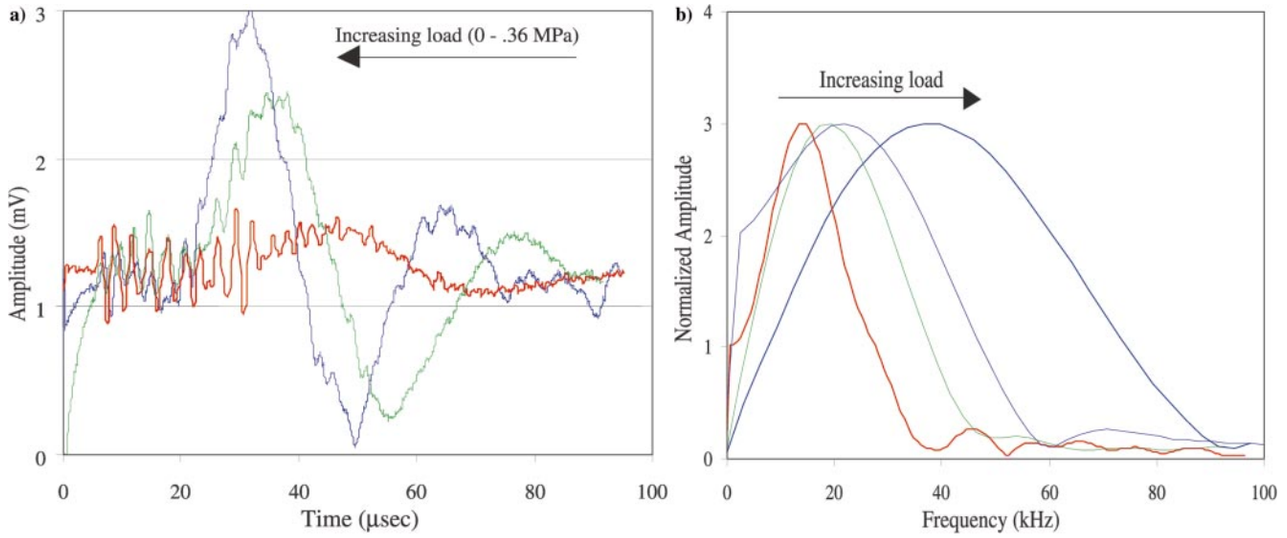

FIG. 6. S-wave signals (a) and their normalized Fourier frequency spectra (b) through water-saturated sands at lowest effective pressures, up to 0.36 MPa. The higher frequency oscillations belong to P-precursor signals. Red curve was made at 0 MPa after the loading cycle. During the loading experiment, no S-signal could be recorded. It was visible only after the loading process was completed and the sand had been precompacted. Note the large difference in wavelength between the signals measured at 0 MPa and at 0.36 MPa.

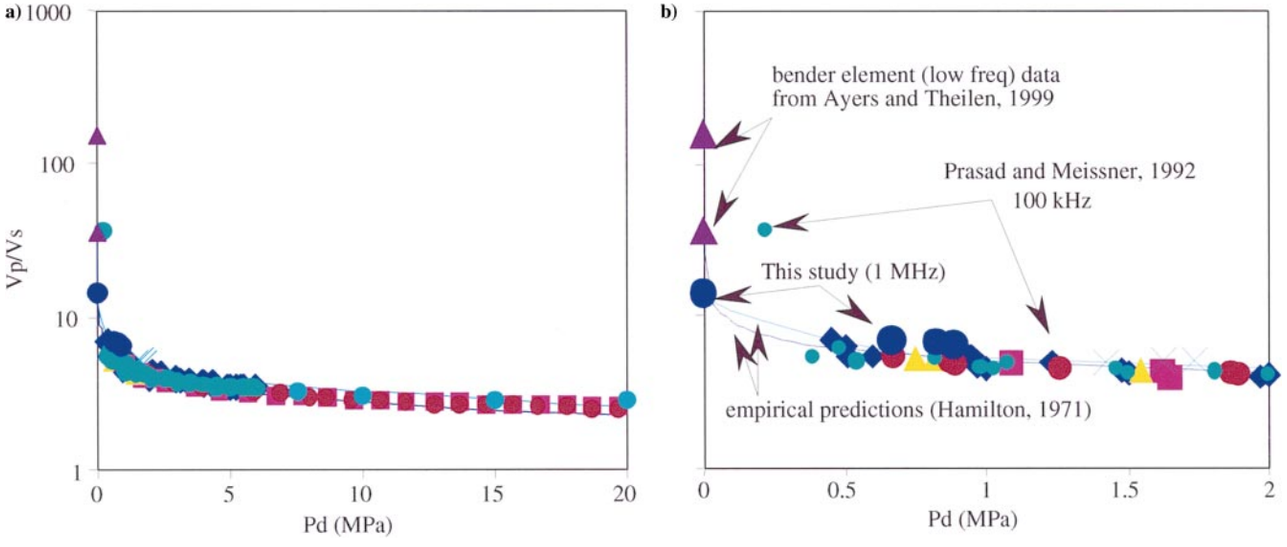

FIG. 7. V_p/V_s ratio for sands measured for this study along with data calculated from measurements by Prasad (1988) and by Ayers and Theilen (1999). The solid lines are calculated from empirical relations for V_p and V_s versus depth given by Hamilton (1971a, b). Figure 7a shows all the data, Figure 7b shows details of the changes in V_p/V_s ratio at low pressures. There is a good agreement between all the data; V_p/V_s ratio increases exponentially at low pressures.

Table 3. Pressure, V_p/V_s, and Poisson's ratio data used in this study. The V_p/V_s and Poisson's ratio values are calculated from the sources in Table 1 and mentioned by acronyms: P88 = Prasad (1988); the numbers P1 to P6 denote grain size. The median grain diameter is given in parenthesis with P1 = coarse (650 μm) and P6 = fine (220 μm) sand; Y92 = Yin (1992); AT99 = Ayers and Theilen (1999); and TS = this study (250–550 μm).

Pressure (MPa)	V_p (m/s)	V_s (m/s)	V_p/V_s	Poisson's ratio	Source
0.000	2962	190	15.4	0.498	TS: coarse sand
0.662	2724	417	6.5	0.488	TS: coarse sand
0.827	2642	421	6.3	0.487	TS: coarse sand
0.883	2633	435	6.1	0.486	TS: coarse sand
0.001	1403	9	155.9	0.500	AT99: marine sediments
0.001	1685	47	35.9	0.500	AT99: marine sediments
5.0	2120	630	3.4	0.452	Y92: sands
7.5	2120	650	3.3	0.448	Y92: sands
7.5	2160	710	3.0	0.439	Y92: sands
10.0	2160	710	3.0	0.439	Y92: sands
10.0	2220	760	2.9	0.434	Y92: sands
15.0	2260	790	2.9	0.430	Y92: sands
15.0	2270	830	2.7	0.423	Y92: sands
20.0	2280	810	2.8	0.428	Y92: sands
20.0	2310	980	2.4	0.390	Y92: sands
30.0	2410	1050	2.3	0.383	Y92: sands
30.0	2440	1070	2.3	0.381	Y92: sands
40.0	2480	1120	2.2	0.372	Y92: sands
40.0	2510	1130	2.2	0.373	Y92: sands
50.0	2540	1260	2.0	0.337	Y92: sands
50.0	2540	1260	2.0	0.337	Y92: sands
0.45	1970	288	6.8	0.489	P88:P1 (650 μm)
0.50	1971	307	6.4	0.488	P88:P1 (650 μm)
0.94	1997	369	5.4	0.482	P88:P1 (650 μm)
0.95	1986	371	5.4	0.482	P88:P1 (650 μm)
1.23	1990	405	4.9	0.478	P88:P1 (650 μm)
2.08	2041	472	4.3	0.472	P88:P1 (650 μm)
2.39	2061	493	4.2	0.470	P88:P1 (650 μm)
2.94	2072	519	4.0	0.467	P88:P1 (650 μm)
3.08	2073	534	3.9	0.464	P88:P1 (650 μm)
3.46	2084	546	3.8	0.463	P88:P1 (650 μm)
4.04	2086	559	3.7	0.461	P88:P1 (650 μm)
4.34	2096	569	3.7	0.460	P88:P1 (650 μm)
4.88	2125	609	3.5	0.455	P88:P1 (650 μm)
5.41	2148	614	3.5	0.456	P88:P1 (650 μm)
5.95	2174	628	3.5	0.454	P88:P1 (650 μm)
1.09	1957	392	5.0	0.479	P88:P2 (550 μm)
1.62	1964	446	4.4	0.473	P88:P2 (550 μm)
2.20	1989	500	4.0	0.466	P88:P2 (550 μm)
0.75	1919	365	5.3	0.481	P88:P3 (460 μm)
0.82	1917	365	5.3	0.481	P88:P3 (460 μm)
1.55	1947	447	4.4	0.472	P88:P3 (460 μm)
1.94	1962	468	4.2	0.470	P88:P3 (460 μm)
0.55	1833	96	19.1	0.499	P88:P4 (360 μm)
0.90	1861	90	20.7	0.499	P88:P4 (360 μm)
1.42	1860	372	5.0	0.479	P88:P4 (360 μm)
1.63	1886	371	5.1	0.480	P88:P4 (360 μm)
1.74	1883	375	5.0	0.479	P88:P4 (360 μm)
0.48	1872	310	6.0	0.486	P88:P5 (300 μm)
0.82	1915	361	5.3	0.482	P88:P5 (300 μm)
1.07	1923	390	4.9	0.479	P88:P5 (300 μm)
1.46	1933	429	4.5	0.474	P88:P5 (300 μm)
1.81	1952	455	4.3	0.471	P88:P5 (300 μm)
2.61	1978	498	4.0	0.466	P88:P5 (300 μm)
3.06	1989	522	3.8	0.463	P88:P5 (300 μm)
3.50	1991	534	3.7	0.461	P88:P5 (300 μm)
3.95	1991	554	3.6	0.458	P88:P5 (300 μm)
4.46	2009	572	3.5	0.456	P88:P5 (300 μm)
5.12	2027	587	3.5	0.454	P88:P5 (300 μm)
5.50	2050	592	3.5	0.455	P88:P5 (300 μm)
5.93	2061	598	3.4	0.454	P88:P5 (300 μm)
0.67	1828	335	5.5	0.483	P88:P6 (220 μm)
0.87	1835	365	5.0	0.479	P88:P6 (220 μm)
1.26	1835	403	4.6	0.475	P88:P6 (220 μm)
1.87	1854	445	4.2	0.469	P88:P6 (220 μm)

(*PR*) are calculated for dry and water-saturated sands underlying a shale cap using equation (1) from Verm and Hilterman (1995):

$$NI = (Ip_2 - Ip_1)/(Ip_2 + Ip_1), \quad \text{and}$$
$$PR = (\nu_2 - \nu_1)/(1 - \nu_{\text{avg.}})^2, \tag{1}$$

where Ip = acoustic impedance, and ν = Poisson's ratio. The subscripts denote the two layers. On the basis of the V_p/V_s ratios and the calculated *NI* and *PR* values, not only can we separate the dry sands from the water-saturated sands, but we can also predict pressure changes within each case.

The relations were derived in this study span a wide frequency range from tens of kilohertz to 1 MHz. Their general conclusion can be assumed to be valid at seismic frequencies as well, with minor effects due to higher shear attenuation and related dispersion since the physical phenomenon underlying these observations is frequency independent.

CONCLUSIONS

The above considerations show that V_p/V_s and Q_p/Q_s ratios can be useful predictors of low differential pressures and can be used as indicators of zones with overpressure. The V_p/V_s ratio can reach values above 100 in conditions of low differential pressures. An empirical relation has been derived for the change in V_p/V_s with pressure; $V_p/V_s = 5.6014 \times P_d^{-0.2742}$ that suggests that high values of V_p/V_s can be expected up to 2 MPa. An analysis of waveforms of *P*- and *S*-waves through unconsolidated sands at low (below 1 MPa) pressure shows that *S*-waves in both velocity and attenuation are very sensitive to pressure. By calculating normal incidence reflectivity and the Poisson reflectivity, not only can we separate between dry and

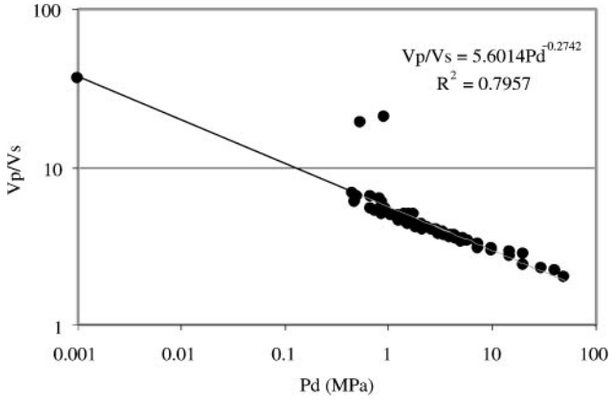

FIG. 8. V_p/V_s ratio for all data on sands from Table 3. There is a clear linear trend of V_p/V_s versus pressure on the log-log plot. An empirical fit through the data (solid line) and the fitting equation is also given. The coefficient of regression for this fit (R^2) is about 0.8.

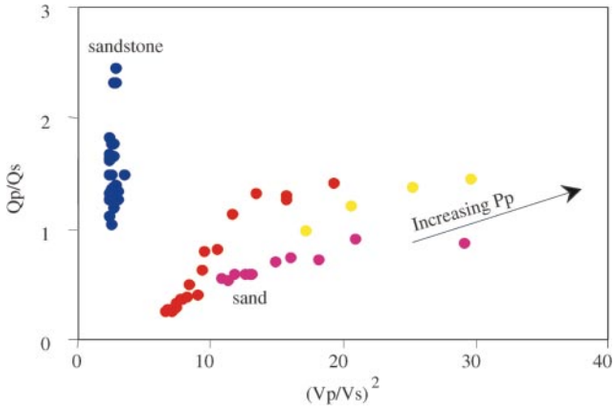

FIG. 9. Q_p/Q_s versus $(V_p/V_s)^2$ for sands from Table 3 compared with sandstones from Prasad (2001). The sandstones and sands plot in different domains. Also shown in the plot is the effect of increasing pore pressure.

Table 4. Pressure, V_p, V_s, V_p/V_s, Poisson's ratio, density, *P*-wave impedance, *NI*, and *PR* for two sands: dry and water saturated. The *NI* and *PR* are calculated for a shale cap. The velocity and Poisson's ratio values for the shale are taken from Verm and Hilterman (1995) and for the sand from Prasad and Meissner (1992).

P_d (MPa)	V_p (m/s)	V_s (m/s)	V_p/V_s	Poisson's ratio	Density (g/cm^3)	Impedance (kg/s × m^2/10^3)	*NI*	*PR*
Shale	2940			0.36	2.33	6850.2		
Water-saturated sand								
0.89	1904	398	4.78	0.48	2.02	3852	−0.28	0.35
2.89	1977	534	3.70	0.46	2.03	4019	−0.26	0.29
5.89	2076	633	3.28	0.45	2.05	4250	−0.23	0.25
8	2088	698	2.99	0.44	2.06	4295	−0.23	0.21
10.65	2088	742	2.81	0.43	2.07	4322	−0.23	0.18
14.67	2122	792	2.68	0.42	2.09	4435	−0.21	0.16
19.67	2157	852	2.53	0.41	2.12	4562	−0.20	0.13
Dry sand								
1.02	747	333	2.24	0.38	1.89	1414	−0.66	0.04
3	903	431	2.10	0.35	1.90	1713	−0.60	−0.02
6.02	1031	555	1.86	0.30	1.90	1962	−0.55	−0.14
8.95	1136	620	1.83	0.29	1.91	2169	−0.52	−0.16
10.2	1185	631	1.88	0.30	1.91	2266	−0.50	−0.13
14.5	1300	696	1.87	0.30	1.92	2497	−0.47	−0.14
19.8	1431	764	1.87	0.30	1.93	2765	−0.42	−0.13

water-saturated sands, but we can also track pressure changes within each formation.

ACKNOWLEDGMENTS

This work is supported by the Stanford Rockphysics and Borehole (SRB) Project. I thank John Castagna, Mike Batzle, Carl Sondergeld, Alan Huffman, and Wayne Pennington for reviewing the manuscript and for their comments. Special thanks to Mike Zimmer for his comments and for continuing this work.

REFERENCES

Ayers, A., and Theilen, F., 1999, Relationship between *P*- and *S*-wave velocities and geological properties of near-surface sediments of the continental slope of the Barents Sea: Geophys. Prosp., **47**, 431–441.

Dutta, N. C., 1987, Geopressure: Soc. Expl. Geophys.

Hamilton, E. L., 1971a, Elastic properties of marine sediments: J. Acoust. Soc. Am., **28**, 16–19.

——— 1971b, Prediction of in situ acoustic and elastic properties of marine sediments: Geophysics, **36**, 266–284.

Hottmann, C. E., and Johnson, R. K., 1965, Estimation of formation pressures from log-derived shale properties: J. Petr. Tech., **17**, 717–722.

Huffman, A. R., and Castagna, J. P., 1999, Rock physics and mechanics considerations for shallow water flow characterization: Shallow Water Flow Conf. Proc.

Huffman, A. R., and Castagna, J. P., 2000, Shallow water flow prediction from seismic analysis of multicomponent seismic data: Offshore Technology Conference, paper 11974.

Nur, A., Mavko, G., Dvorkin, J., and Gal, D., 1995, Critical porosity: The key to relating physical properties to porosity in rocks: 65th Ann. Internat. Mtg., Soc. Expl. Geophys., Expanded Abstracts, 878–879.

Pennebaker, E. S., Jr., 1970, A drilling engineering interpretation of seismic field data: Soc. Petr. Eng., Am. Inst. Min., Metall. Petr. Eng. Meeting, SPE paper 2165.

Pilkington, P. E., 1988, Uses of pressure and temperature data in exploration and new developments in overpressure detection: J. Petr. Tech., **40**, 543–549.

Prasad M., 1988, Experimental and theoretical considerations of velocity and attenuation interactions with physical parameters in sands: Ph.D. thesis, Kiel University.

——— 2001, Mapping impedance microstructures in rocks with acoustic microscopy: The Leading Edge, **20**, 172–179.

Prasad M., and Meissner, R., 1992, Attenuation mechanisms in sands: Laboratory versus theoretical (Biot) data: Geophysics, v. **57**, 710–719.

Verm, R., and Hilterman, F., 1995, Lithology color-coded seismic sections: The calibration of AVO crossplotting to rock properties: The Leading Edge, **14**, 847–853.

Winkler, K. W., 1983, Contact stiffness in granular porous materials. Comparison between theory and experiments: Geophy. Res. Lett., **10**, 1073–1076.

Yin, H., 1992, Acoustic velocity and attenuation of rocks: Isotropy, intrinsic anisotropy, and stress induced anisotropy: Ph.D. thesis, Stanford University.

Zimmer, M., Prasad, M., and Mavko, G., 2002, Pressure and porosity influences on V_p-V_s ratios in unconsolidated sands: The Leading Edge, **21**, 178–183.